IEEE Photonics Journal
An IEEE Photonics Society Publication



# Sequential Shift Absolute Phase Aberration Calibration in Digital Holographic Phase Imaging Based on Chebyshev Polynomials Fitting

Volume 12, Number 1, February 2020

Weilin He
Jiantai Dou
Zhongming Yang
Zhenhua Liu
Zhaojun Liu

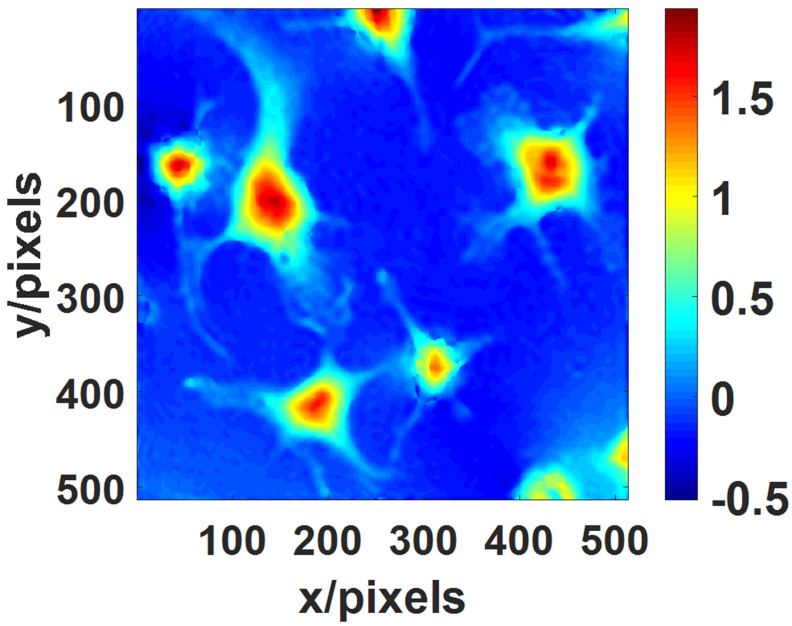


DOI: 10.1109/JPHOT.2019.2953198

# Sequential Shift Absolute Phase Aberration Calibration in Digital Holographic Phase Imaging Based on Chebyshev Polynomials Fitting

**Weilin He,[1] Jiantai Dou,[2] Zhongming Yang,[1] Zhenhua Liu,[3] and Zhaojun Liu [1]**

[1]Shandong Provincial Key Laboratory of Laser Technology and Application, School of Information Science and Engineering, Shandong University, Jinan 250100, China
[2]Department of Physics, College of Science, Jiangsu University of Science and Technology, Zhenjiang 212003, China
[3]Environment Research Institute, Shandong University, Jinan 266237, China

*DOI:10.1109/JPHOT.2019.2953198*


Manuscript received October 7, 2019; revised November 4, 2019; accepted November 8, 2019. Date of publication November 12, 2019; date of current version January 7, 2020. This work was supported in part by the Natural Science Foundation of Shandong Province under Grant ZR2019QF013, in part by the China Postdoctoral Science Foundation under Grant 2018M630773, in part by the Opening Project of CAS Key Laboratory of Astronomical Optics and Technology, Nanjing Institute of Astronomical Optics and Technology under Grant CAS-KLAOT-KF201804, in part by the Open Project Program of Jiangsu Key Laboratory of Spectral Imaging and Intelligent Sense under Grant 3091801410413, and in part by the Fundamental Research Funds of Shandong University under Grant 11170077614092. Corresponding author: Zhongming Yang (e-mail: zhongming.yang@sdu.edu.cn).

**Abstract:** We propose a novel absolute calibrate method for digital holographic microscopy with the sequential shift method using Chebyshev polynomials. We separate the object phase and the aberrations by sequential shifting the sample twice in vertical plane of the optical axis. The aberrations phase is then calculated using the high order Chebyshev polynomials. The correct phase is obtained by subtracting the aberrations from the original phase containing the aberration. This method can compensate for the complex aberrations including high-order aberrations without changing the traditional optical system. Meanwhile, it can effectively protect the medium and high frequency information of the specimen in the phase image. Numerical simulation and experimental results demonstrate the availability and advantages of the absolute calibrate method.

**Index Terms:** Aberration compensation, digital holography, interference microscopy, phase measurement.

## 1. Introduction

Digital holographic microscopy is a nondestructive, label-free, and interferometric quantitative phase-contrast technique, which has an enormous impact in many fields such as biology [1], [2], neural science [3], nanoparticle tracking [4], microfluidics [5], and metrology [6]. Just like other traditional interferometric system, digital holographic microscopy system suffers from the system phase aberrations, which is mainly introduced by the microscopy objective and other optical elements. Generally, the system phase aberrations are superposed over the specimen phase information, which needs to be compensated.

Recently, a lot of physical and numerical methods have been proposed to compensate or calibrate the system phase aberrations. Using the telecentric configuration or tunable lens can introduce the phase aberrations into the reference beam, which will partially compensate the lower order phase aberrations [7], [8]. The double exposure method needs removal the specimen from reference beam in second exposure, and can compensate the total aberrations accurately [9]. In numerical compensation method, the system phase aberrations are descripted by spherical function, parabolic function, and Zernike or Chebyshev polynomials [10]–[13]. Least square fitting method [14] and principal component analysis method could be used to acquire the lower order parameters of the standard polynomials [15], [16]. In fitting methods, the specimen-free area needs to be selected before least square fitting, and the deep learning technique is utilized to select the specimen-free area in recent literature [17]. The phase aberrations also can be extracted in a nonlinear optimization process, the phase variation of specimen as the optimization object [18]. In our previous work, we have developed an automatic high order aberrations correction method based on orthonormal polynomials fitting over irregular shaped aperture [19], however, the calculation time is longer large when the profile of the sample being tested was complex. We have also proposed a method based on the Self-extension of holograms [20], but it is only suitable for the case where the sample distribution is sparse and the sample and background are easily distinguished.

In optical surface metrology, the widely used Fizeau and Twyman-Green interferometers used a normal quality reference surface ($\lambda$/20 Peak to Valley) as a standard in testing, in order to get the subnanometer metrology, the absolute testing technique is one of the most important techniques to calibrate the reference surface deviation. Several absolute testing methods have been proposed for optical surface metrology, such as two sphere method [21], random ball averaging method [22], and shift-rotation method [23]–[28]. In shift-rotation absolute testing method, the position of the reference surface in the measurement process is unchanged, and the test surface is tested in shift and rotation position. Based on the measurement data in shift and rotation position, the deviation of test surface can be extracted. The calibration process of the reference surface deviation in shift-rotation absolute testing method gave us a novel approach to absolute calibration for digital holographic microscopy.

In this paper, we present a novel absolute calibrate method for digital holographic microscopy with the sequential shift method using Chebyshev polynomials. Three holograms were captured while moving the sample twice in two orthogonal directions perpendicular to the optical axis. The key point of our work is to acquire the aberration parameters of Chebyshev polynomials from these three holograms, in which the phase aberrations can be expressed by a series of Chebyshev polynomials, accordingly. And then, the calculated phase aberrations is subtracted from the phase distribution of the object wave to achieve quantitative phase imaging. The main advantage of the absolute calibration method is that it can effectively protect the medium and high frequency information of the object phase, even for very complex aberrations, can eliminate various low-order and high-order aberrations. Furthermore, the compensation can be achieved for any traditional optical system of digital holographic microscopy. It is simple, accurate, and requires only an additional three-axis stage for a standard experimental setup. In the following sections, the theory of absolute calibrate method is discussed, and the technique is then demonstrated by numerical simulation and experiment.

## 2. Principle

Zernike polynomials are widely used in phase aberrations analysis for their orthogonality over a unit circular aperture and representation of classical aberrations in the optical system. But Zernike polynomials lose orthogonality in square apertures, for the digital hologram with a square and rectangular aperture, the non-orthogonality of Zernike polynomials results in its unsuitable for representation of system phase aberrations in digital holographic microscopy, it needs to be transformed to satisfy the orthogonality on the square aperture to apply to the square aperture hologram. [19] However, Chebyshev polynomials are orthogonal over square aperture, the phase aberrations

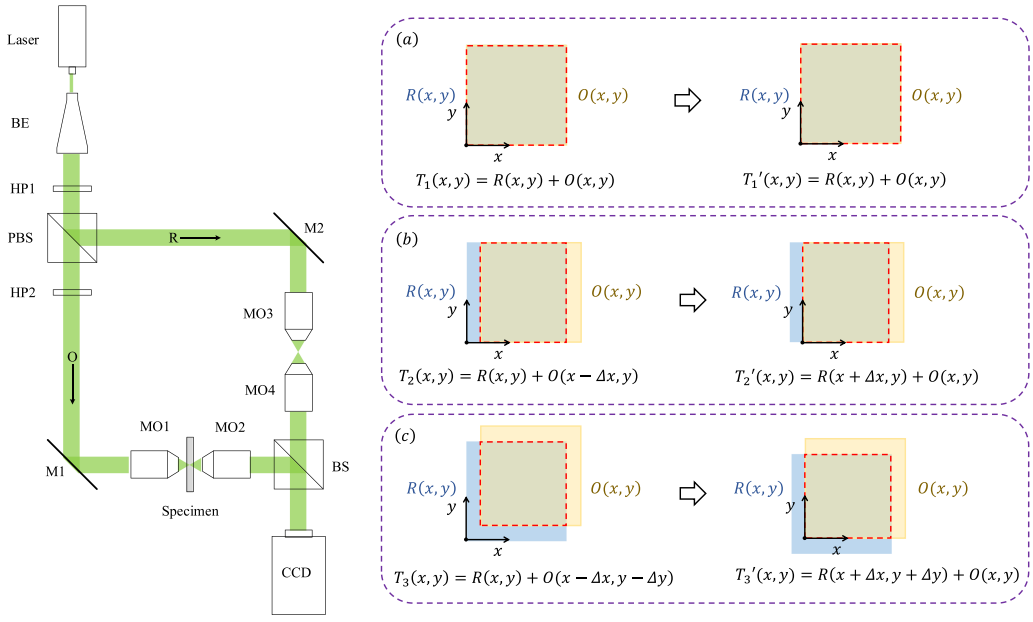


Fig. 1. The absolute calibration process. (a) Basic position, (b) $x$ direction translation position, (c) $y$ direction translation position.

in digital hologram can be represented by a sum of Chebyshev terms, and the coefficients of the Chebyshev polynomials are the unknown quantities. The phase map of captured digital hologram can be expressed as:

$$T(x, y) = R(x, y) + O(x, y) \tag{1}$$

where $O(x, y)$ is the phase map of the test object, $R(x, y)$ is the phase aberration of the digital holographic microscopy, which can be represented by:

$$R(x, y) = \sum_{i=1}^{n} a_i C_i(x, y) \tag{2}$$

where $a_i$ are the coefficients of Chebyshev polynomials, $C_i(x, y)$ are the Chebyshev terms, and $n$ is the number of the Chebyshev terms.

The sequential shift absolute calibrate method using Chebyshev polynomials is based on the relative testing of the phase map of the test object $O(x, y)$ and the phase aberration of the digital holographic microscopy $R(x, y)$. The specimen is tested in two sequential shift positions, the measurement process is shown in Fig. 1. First, the specimen is tested in the original position, the measurement result is:

$$T_1(x, y) = R(x, y) + O(x, y) \tag{3}$$

The coordinate system is unchanged in original position, after the coordinate system translated, the calculation result is:

$$T_1'(x, y) = R(x, y) + O(x, y) = \sum_{i=1}^{n} a_i C_i(x, y) + O(x, y) \tag{4}$$

And then, the specimen is translated a distance in $x$ direction, the measurement results is:

$$T_2(x, y) = R(x, y) + O(x - \Delta x, y) \tag{5}$$

The coordinate system is translated in opposite direction, after the coordinate system translated in $x$ direction translation position, the calculation result is:

$$T_2'(x,y) = R(x+\Delta x, y) + O(x,y) = \sum_{i=1}^{n} a_i C_i(x+\Delta x, y) + O(x,y) \tag{6}$$

At last, the specimen is translated a distance in $y$ direction, the measurement results is:

$$T_3(x,y) = R(x,y) + O(x-\Delta x, y-\Delta y) \tag{7}$$

The coordinate system is translated in opposite direction, after the coordinate system translated in $y$ direction translation position, the calculation result is:

$$T_3'(x,y) = R(x+\Delta x, y+\Delta y) + O(x,y) = \sum_{i=1}^{n} a_i C_i(x+\Delta x, y+\Delta y) + O(x,y) \tag{8}$$

After the coordinate system is translation, the phase map of the test object $O(x, y)$ is unchanged during the measurement. Using the Eq. (6) and Eq. (8) minus Eq. (4), we can get the differential data of the phase aberration of the digital holographic microscopy $R(x, y)$ between the translation positions and original position. We can get:

$$\begin{cases} \Delta T_1(x,y) = \sum_{i=1}^{n} a_i \Delta C_{ix}(x,y) \\ \Delta T_2(x,y) = \sum_{i=1}^{n} a_i \Delta C_{iy}(x,y) \end{cases} \tag{9}$$

where $\Delta C_{ix}(x, y)$ and $\Delta C_{iy}(x, y)$ are differential of the Chebyshev polynomials in $x$ and $y$ direction. The Eq. (9) can be expressed in matrix form as:

$$CA = \Delta T \tag{10}$$

where $C$, $A$, and $\Delta T$ are expressed as:

$$C = \begin{bmatrix} \Delta C_{1x}(1,1) & \Delta C_{2x}(1,1) & \cdots & \Delta C_{nx}(1,1) \\ \Delta C_{1x}(1,2) & \Delta C_{2x}(1,2) & \cdots & \Delta C_{nx}(1,2) \\ \cdots & \cdots & \cdots & \cdots \\ \Delta C_{1x}(M,N) & \Delta C_{2x}(M,N) & \cdots & \Delta C_{nx}(M,N) \\ \Delta C_{1y}(1,1) & \Delta C_{2y}(1,1) & \cdots & \Delta C_{ny}(1,1) \\ \Delta C_{1y}(1,2) & \Delta C_{2y}(1,2) & \cdots & \Delta C_{ny}(1,2) \\ \cdots & \cdots & \cdots & \cdots \\ \Delta C_{1y}(M,N) & \Delta C_{2y}(M,N) & \cdots & \Delta C_{ny}(M,N) \end{bmatrix} \tag{11}$$

$$A = \begin{bmatrix} a_1 & a_2 & \cdots & a_n \end{bmatrix}^T \tag{12}$$

$$\Delta T = \begin{bmatrix} \Delta T_1(1,1) & \Delta T_1(1,2) & \cdots & \Delta T_1(M,N) & \Delta T_2(1,1) & \Delta T_2(1,2) & \cdots & \Delta T_2(M,N) \end{bmatrix}^T \tag{13}$$

where $M$ and $N$ are the number of rows and columns of the digital hologram. Solving the Eq. (10), the coefficients of Chebyshev polynomials $a_i$ can be obtained, the phase aberration of the digital holographic microscopy $R(x, y)$ can be calculated by Eq. (2). That is, the aberration distribution is obtained by using a Chebyshev polynomial that satisfies the orthogonality on the square aperture.

## 3. Numerical Simulation and Analysis

In order to validate the accuracy and feasibility of the proposed absolute calibration for digital holographic microscopy with the sequential shift method using Chebyshev polynomials, the phase map of the test object $O(x, y)$ in literature [14] are used in our numerical simulation, which has remove the lower order phase aberration by the principal component analysis. The digital

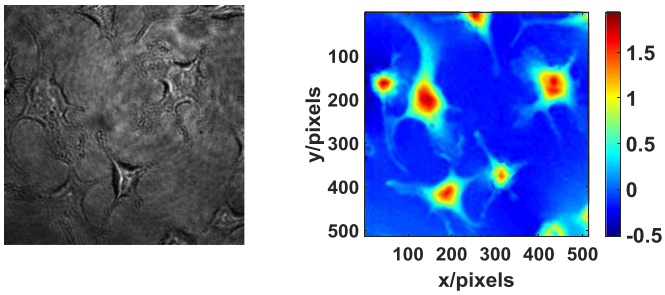


Fig. 2. Specimen phase data in numerical simulation (units: rad). (a) The digital hologram of specimen. (b) The phase map of specimen after removed the lower order aberrations.

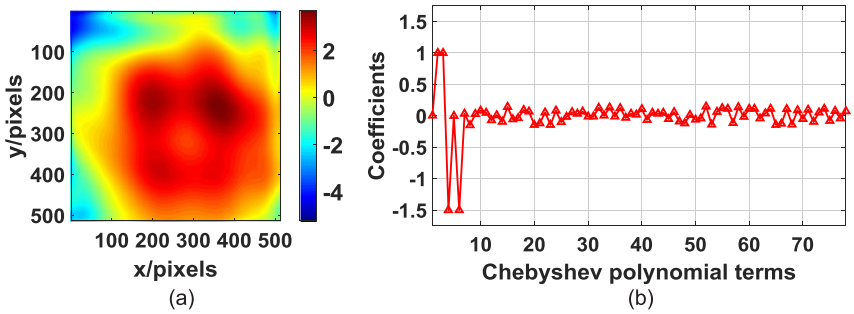


Fig. 3. The phase aberrations in numerical simulation (units: rad). (a) The phase aberrations are generated by the sum of 78 terms Chebyshev polynomials. (b) The coefficients of Chebyshev polynomials of phase aberrations.

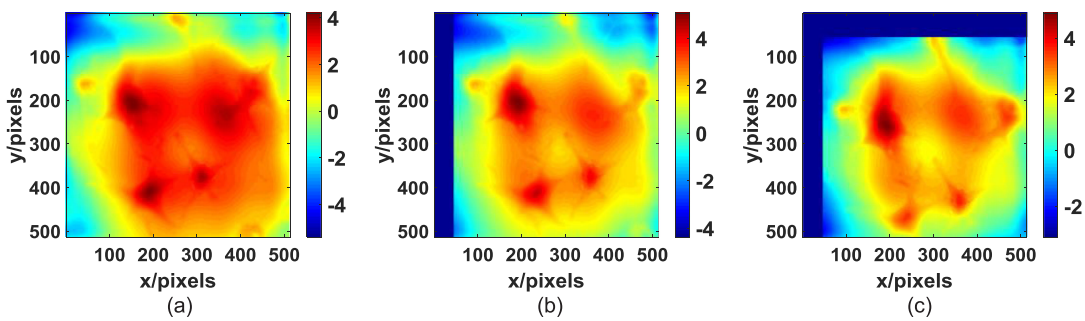


Fig. 4. The measurement results on the three positions in numerical simulation (units: rad). (a) Basic position, (b) $x$ direction translation position, (c) $y$ direction translation position.

hologram is shown in Fig. 2(a) and the phase map of the specimen is shown in Fig. 2(b). For digital holographic phase imaging, the 78-term polynomial is sufficient to include low-order and most high-order aberrations, so the 78-item Chebyshev polynomial is used to generate the phase difference $R(x, y)$ as shown in Fig. 3(a), and the coefficients of Chebyshev polynomials of phase aberrations $R(x, y)$ are shown in Fig. 3(b). Based on the absolute calibration process of phase aberrations described in Section 2, the measurement results on the three positions are shown in Fig. 4. In which, the specimen shifts 46 pixels in $x$ direction and then shifts 58 pixels in $y$ direction. The blue margins in Fig. 4 represents the shifts, which is invalid data. After the coordinate system translation, the measurement results on the three positions are shown in Fig. 5. The differential data of the phase aberration between two translation positions and basic position

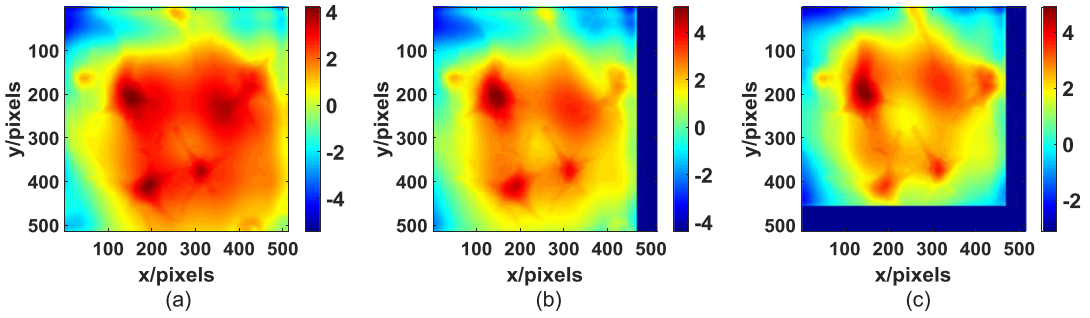


Fig. 5. The measurement results on the three positions after the coordinate system translation in numerical simulation (units: rad). (a) Basic position, (b) *x* direction translation position, (c) *y* direction translation position.

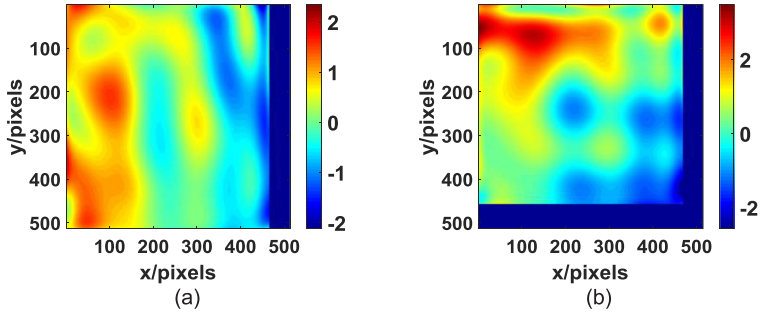


Fig. 6. The differential data of the phase aberration in numerical simulation (units: rad). (a) Between *x* direction translation position and basic position, (b) between *y* direction translation position and basic position.

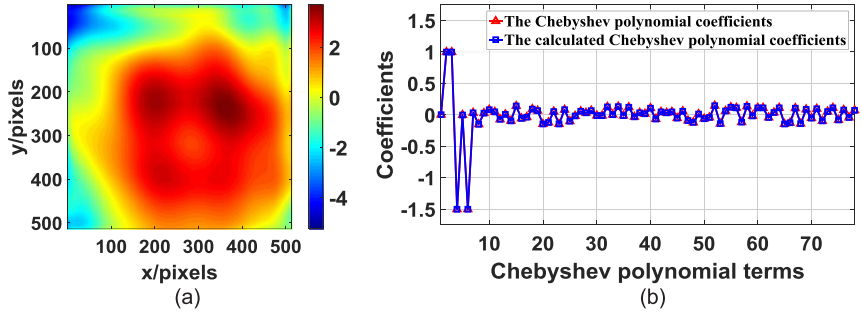


Fig. 7. The phase aberrations calibrated in numerical simulation (units: rad). (a) The phase aberrations are generated by the sum of 78 terms Chebyshev polynomials. (b) The calculated Chebyshev polynomials coefficients of the phase aberrations compared with the Chebyshev polynomials coefficients of simulated phase aberrations.

are shown in Fig. 6, respectively. Based on Eq. (10), the phase aberrations calibrated in the numerical simulation is shown in Fig. 7(a), which is described by the coefficients of the Chebyshev polynomials $a_i$. The calculated Chebyshev polynomial coefficients and the Chebyshev polynomial coefficients set by simulation are compared in Fig. 7(b). The difference between the calculated phase aberration and the set aberration is as shown in Fig. 8. It can be seen that (the absolute calibration of) the proposed sequential shift method using Chebyshev polynomials has calibrated the high-order and low-order phase aberrations in digital holographic microscopes.

In theory, even very small displacements can satisfy the theoretical requirements, but for CCDs and algorithms, 1 pixel is the smallest unit that can be resolved, so 1 pixel distance is the minimum

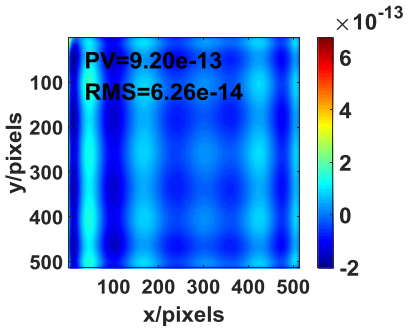


Fig. 8. The calibrated error of phase aberrations in numerical simulation (units: rad).

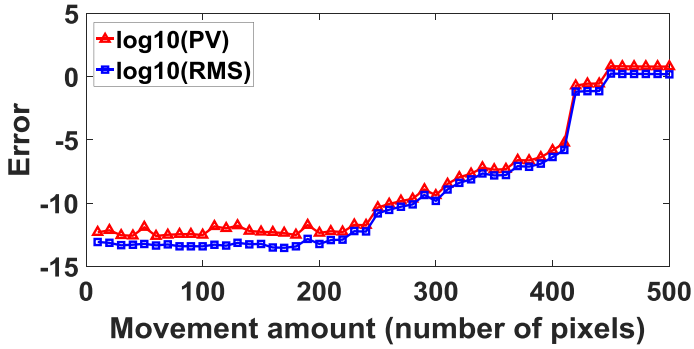


Fig. 9. The relationship between the calibration error of phase distortion and the amount of movement in numerical simulation.

moving distance that satisfies the algorithm. However, the algorithm needs to convert the actual moving distance into a value in pixels that must be an integer. This conversion process will inevitably lead to errors. This error value is smaller than the side length of a single pixel, so the moving distance needs to be larger, so that the error value is relatively small. However, the moving distance should not be too large. As shown in Fig. 1(c), the effective area used by the algorithm is a red dashed box, the algorithm compensates for the aberrations by solving the polynomial coefficients of the aberrations from the region in the red dotted frame. If the moving distance is too large, the effective area will become smaller and the error of the algorithm will increase, and when the amount of movement is large enough, the algorithm will not even get valid results.

As shown in Fig. 8, when the movement amount is 46 pixels on the x-axis and 58 pixels on the y-axis, the calibration error of the phase distortion is PV = 1.6298e-12 and RMS = 6.6393e-14, as shown in Fig. 9, the larger the amount of movement, the larger the calculation error.

## 4. Experiments and Results

To verify the performance of the absolute calibrate method, we performed verification experiments using paramecium microsections. Fig. 1 shows the schematic setup based on the Mach-Zehnder interferometer. The linearly polarized laser beam ($\lambda = 632.8$ nm) is expanded by a beam expander. The object beam passes through the sample and meets the reference beam at the beam splitter. Both the object beam and the reference beam are amplified by the microscope objective and produce interference fringes on the CCD for digital recording. The micro-displacement of the sample is achieved by a three-axis stage. The three-axis stage is fixed on the optical table by nuts and the sample is clamped during the measurement process to prevent the natural movement due to the looseness of the fixture. The experiment used a regular PC (CPU 2.3 GHz RAM 12 GB).

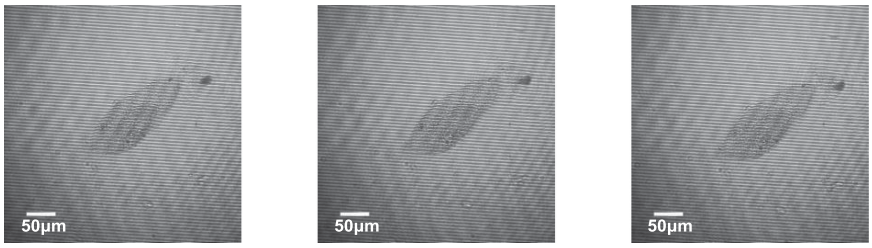


(a) (b) (c)

Fig. 10. The hologram of the paramecium. (a) Hologram of paramecium in its original position. (b) Hologram of paramecium moving in the x-axis direction (23 pixels). (c) Hologram of paramecium moving in the y-axis direction (25 pixels).

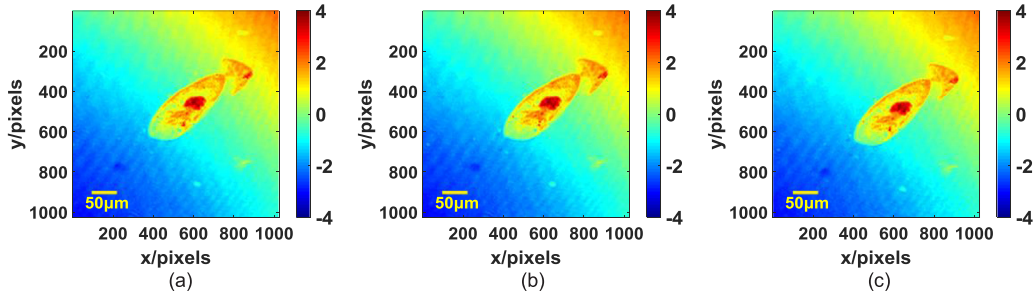


Fig. 11. The phase of the paramecium with aberrations. (a)-(c) is the phase corresponding to (a)-(c) in Fig. 10, respectively.

After simulation and experiment, the amount of movement we selected in the experiment is about 10 microns, corresponding to the distance of the pixel distance is 23 pixels on the x-axis and 25 pixels on the y-axis. Limited to the experimental conditions, we did not do a strict calibration, so this is not a strict conversion ratio of the actual distance to the number of pixels. In this situation, the difference distance between the moving pixel distance and the actual moving distance is relatively small. If the moving pixel distance is additionally introduced into a 1-pixel count error, there will be no detectable change in the result. That is to say, the error between the actual moving distance and the moving pixel distance is small and can be ignored. Meanwhile, the moving distance is small relative to the entire field of view, so the effective area occupies most of the entire hologram and the error of the algorithm is small.

The numerical reconstruction steps are depicted in Fig. 1. We first get the first hologram where the sample is in the original position, as shown in Fig. 10(a). Then move the sample in the x-axis direction (23 pixels) and get the second hologram, as shown in Fig. 10(b). Finally, move the sample in the y-axis direction (25 pixels) and get the third hologram, as shown in Fig. 10(c). The captured digital holograms were processed according to the phase demodulation method based on Fourier transform to obtain the phase distribution map corresponding to the three holograms, as shown in Fig. 11. The double fringes along two diagonal directions in Fig. 10 are caused by stray light that is reflected back and forth between the optical elements which caused the ripple error along the two diagonal directions in Fig. 11. The circular bright aperture in the figures (a)(b) and (c) is because the light source used in the experiment is a Gaussian beam, which is not completely uniform even after spatial filtering and beam collimation. Therefore, the middle part of the beam will be brighter, while the edge of the beam will be slightly darker. However, the difference between the brightness of the center of the beam and the edge is small and does not affect the sharpness of the fringes, so it does not affect the phase measurement in the algorithms used. Fig. 12 shows the aberrations distribution obtained by the absolute calibrate method and the phase distribution of the paramecium

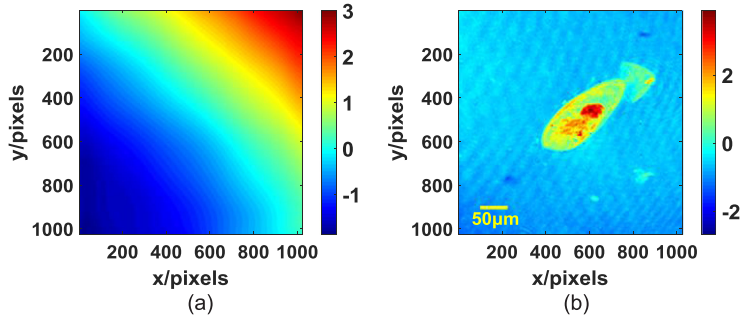


Fig. 12. The result of the absolute calibrate method. (a) The aberration obtained by the absolute calibrate method. (b) The paramecium phase obtained by the absolute calibrate method.

TABLE 1
The Time Cost of PCA Based Method, Self-Extension Based Method and the Absolute Detection Method

| | PCA based method | Self-extension based method | The absolute detection method |
|---|---|---|---|
| Time (s) | 5.09 | 54.33 | 81.98 |

after compensating for aberrations. The result proves that the absolute calibrate method works well to compensate for aberrations.

To further examine the performance of the absolute calibrate method, we use the principal component analysis based method described in references 14, 15, and our previous method based on the Self-extension of holograms described in references 20 for phase extraction and aberration compensation of the hologram. Fig. 13 demonstrates the experimental results of retrieved phase distributions with these three methods. We mark a small area containing the paramecium at the same location in Fig. 13(a), (b) and (c) using a yellow box. The retrieved phase part in the yellow box part of Fig. 13(a), (b) and (c) is shown in Fig. 13(d), (e) and (f), respectively. In order to observe and contrast these three methods more intuitively, the cross-sectional profile of the yellow line along the same position in Fig. 13(d), (e) and (f) is given in Fig. 13(g). The time cost of these three methods is shown in Table 1.

We noticed that the PCA based method takes the shortest time, while the absolute detection method takes the longest time, and all the three methods are good for aberration compensation. It can be seen from Fig. 13(g) that the tendency of the profile lines taken by the three are quite similar. However, comparing the correction result in Figs. 13(a), 13(d) and Figs. 13(b), 13(e) with that in Figs. 13(c), 13(f), it is obvious that the results of the principal component analysis method and the Self-extension based method are relatively ambiguous, and its profile lines is smoother, with some peaks fluctuating less or merging with adjacent peaks. This illustrates the fact that the principal component analysis method and the Self-extension based method suffer from the uncertainty of the loss of sample detail phase information. This difference arises from the fact that the principal component analysis method extracts and compensates aberrations by filtering in the frequency domain, which inevitably leads to the loss of a little bit of sample detail phase information. The Self-extension based method removes the fringes in the sample area and then recovers the hologram by self-expansion, which also results in loss of information.

The absolute detection method is to first separate the phase of the object and the aberrations by shifting the sample twice. The aberrations phase is then calculated using a Chebyshev polynomial. Due to the superiority of Chebyshev polynomials in characterizing aberrations, the absolute detection method can better preserve object information, and give a relatively cleaner phase images result. However, compared to principal component analysis and the Self-extension based method, the absolute detection method has an extra holistic displacement due to the glass slides of the paramecium. It is arises from the characteristic that the phase information of the object

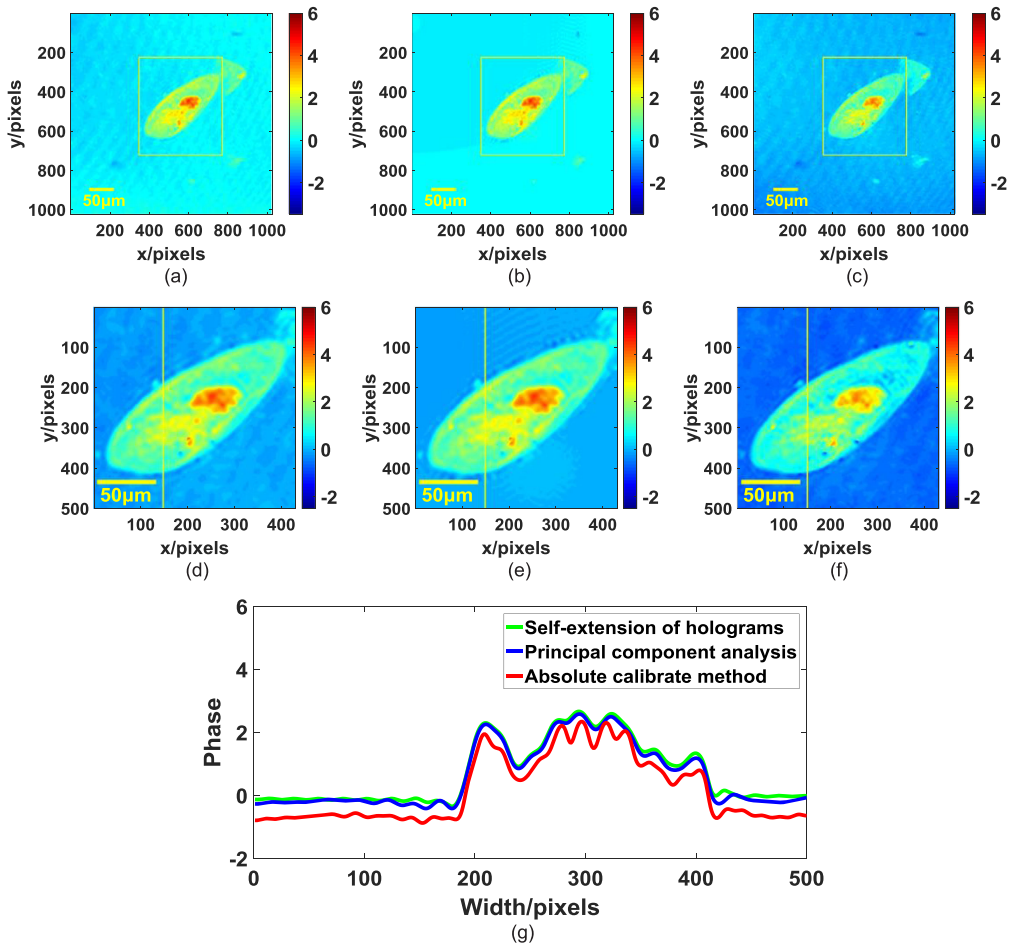


Fig. 13. (a) The phase compensation result of the principal component analysis based method. (b) The phase compensation result of the Self-extension based method. (c) The phase compensation result of the absolute calibrate method. (d), (e) and (f) is the enlarged area marked in (a), (b) and (c), respectively. (g) The cross-sectional profile of the yellow line mark in (d), (e) and (f).

is composed of paramecium and glass slides in the absolute detection method, so the phase result of aberration compensation is also composed of paramecium and glass slides. That is, the result phase is equivalent to adding an approximate constant to the phase of paramecium.

## 5. Summary

In conclusion, we have presented a novel absolute calibrate method for phase aberration correction in digital holographic microscopy with the sequential shift method using Chebyshev polynomials. The method is based on Chebyshev polynomial aberration fitting. The compensation is performed through an automatic procedure which needs three special holograms. Since there is no filtering in the frequency domain, absolute calibration method better preserves high frequency information of samples compared to other numerical fitting methods. In addition, our method can compensate for sample phase aberrations of any complexity, such as dense sample distribution or even when the sample fills the entire view. Moreover, since the 78-item Chebyshev polynomial contains low-order and most high-order aberrations, this method can compensate for all low-order and high-order aberrations even in the case where the aberration is very complicated. Simulations and experiments demonstrate the effectiveness and advantages of this approach.

## References


[1] B. Rappaz *et al.*, "Noninvasive characterization of the fission yeast cell cycle by monitoring dry mass with digital holographic microscopy," *J. Biomed. Opt.*, vol. 14, no. 3, May 2009, Art. no. 034049.

[2] Y. Fang *et al.*, "Investigating dynamic structural and mechanical changes of neuroblastoma cells associated with glutamate-mediated neurodegeneration," *Sci. Rep.*, vol. 4, Nov. 2014, Art. no. 7074.

[3] N. Pavillon *et al.*, "Cell morphology and intracellular ionic homeostasis explored with a multimodal approach combining epifluorescence and digital holographic microscopy," *J. Biophotonics*, vol. 3, no. 7, pp. 432–436, Jul. 2010.

[4] N. Warnasooriya *et al.*, "Imaging gold nanoparticles in living cell environments using heterodyne digital holographic microscopy," *Opt. Exp.*, vol. 18, no. 4, pp. 3264–3273, Feb. 2010.

[5] V. P. Pandiyan and R. John, "Optofluidic bioimaging platform for quantitative phase imaging of lab on a chip devices using digital holographic microscopy," *Appl. Opt.*, vol. 55, no. 3, pp. A54–59, Jan. 2016.

[6] E. Cuche, P. Marquet, and C. Depeursinge, "Simultaneous amplitude-contrast and quantitative phase-contrast microscopy by numerical reconstruction of Fresnel off-axis holograms," *Appl. Opt.*, vol. 38, no. 34, pp. 6994–7001, Dec. 1999.

[7] C. Trujillo, R. Castañeda, P. Piedrahita-Quintero, and J. Garcia-Sucerquia, "Automatic full compensation of quantitative phase imaging in off-axis digital holographic microscopy," *Appl. Opt.*, vol. 55, no. 36, pp. 10299–10306, Dec. 2016.

[8] D. Deng *et al.*, "Simple and flexible phase compensation for digital holographic microscopy with electrically tunable lens," *Appl. Opt.*, vol. 56, no. 21, pp. 6007–6014, Jul. 2017.

[9] P. Ferraro *et al.*, "Compensation of the inherent wave front curvature in digital holographic coherent microscopy for quantitative phase-contrast imaging," *Appl. Opt.*, vol. 42, no. 11, pp. 1938–1946, Apr. 2003.

[10] J. Di, J. Zhao, W. Sun, H. Jiang, and X. Yan, "Phase aberration compensation of digital holographic microscopy based on least squares surface fitting," *Opt. Commun.*, vol. 282, no. 19. pp. 3873–3877, 2009.

[11] J. Min, B. Yao, S. Ketelhut, C. Engwer, B. Greve, and B. Kemper, "Simple and fast spectral domain algorithm for quantitative phase imaging of living cells with digital holographic microscopy," *Opt. Lett.*, vol. 42, no. 2, pp. 227–230, Jan. 2017.

[12] J. Du, Z. Yang, Z. Liu, and G. Fan, "Three-step shift-rotation absolute measurement of optical surface figure with irregular shaped aperture," *Opt. Commun.*, vol. 426, pp. 589–597, Nov. 2018.

[13] J. Öhman and M. Sjödahl, "Improved particle position accuracy from off-axis holograms using a Chebyshev model," *Appl. Opt.*, vol. 57, pp. A157–A163, Jan. 2018.

[14] L. Miccio *et al.*, "Direct full compensation of the aberrations in quantitative phase microscopy of thin objects by a single digital hologram," *Appl. Phys. Lett.*, vol. 90, no. 4, Jan. 2007, Art. no. 041104.

[15] C. Zuo, Q. Chen, W. Qu, and A. Asundi, "Phase aberration compensation in digital holographic microscopy based on principal component analysis," *Opt. Lett.*, vol. 38, no. 10, pp. 1724–1726, May 2013.

[16] J. Sun, Q. Chen, Y. Zhang, and C. Zuo, "Optimal principal component analysis-based numerical phase aberration compensation method for digital holography," *Opt. Lett.*, vol. 41, no. 6, pp. 1293–1296, Mar. 2016.

[17] T. Nguyen, V. Bui, V. Lam, C.B. Raub, L.-C. Chang, and G. Nehmetallah, Automatic phase aberration compensation for digital holographic microscopy based on deep learning background detection, *Opt. Exp.*, vol. 25, pp. 15043–15057, 2017.

[18] S. Liu, Q. Lian, Y. Qing, and Z. Xu, "Automatic phase aberration compensation for digital holographic microscopy based on phase variation minimization," *Opt. Lett.*, vol. 43, no. 8, pp. 1870–1873, Apr. 2018.

[19] Z. Yang, Z. Liu, W. He, J. Dou, X. Liu, and C. Zuo, "Automatic high order aberrations correction for digital holographic microscopy based on orthonormal polynomials fitting over irregular shaped aperture," *J. Opt.*, vol. 21, no. 4, Mar. 2019, Art. no. 045609.

[20] W. He, Z. Liu, Z. Yang, J. Dou, X. Liu,and Y. Zhang, "Robust phase aberration compensation in digital holographic microscopy by self-extension of holograms," *Opt. Commun.*, vol. 445, pp. 69–75, Aug. 2019.

[21] K. Creath and J. C. Wyant, "Testing spherical surfaces: A fast, quasi-absolute technique," *Appl. Opt.*, vol. 31, no. 22, pp. 4350–4354, Aug. 1992.

[22] U. Griesmann, Q. Wang, J. Soons, and R. Carakos, "A simple ball averager for reference sphere calibrations," in *Proc. Opt. Manuf. Testing VI*, 2005, vol. 5869, Art. no. 58690S.

[23] E. E. Bloemhof, "Absolute surface metrology by differencing spatially shifted maps from a phase-shifting interferometer," *Opt. Lett.*, vol. 35, no. 14, pp. 2346–2348, Jul. 2010.

[24] D. Su, E. Miao, Y. Sui, and H. Yang, "Absolute surface figure testing by shift-rotation method using Zernike polynomials," *Opt. Lett.*, vol. 37, no. 15, pp. 3198–3200, Aug. 2012.

[25] W. Song, X. Hou, F. Wu, and Y. Wan, "Simple and rapid data-reduction method with pixel-level spatial frequency of shift-rotation method," *Appl. Opt.*, vol. 52, no. 24, pp. 5974–5978, Aug. 2013.

[26] Z. Yang, J. Du, C. Tian, J. Dou, Q. Yuan, and Z. Gao, "Generalized shift-rotation absolute measurement method for high-numerical-aperture spherical surfaces with global optimized wavefront reconstruction algorithm," *Opt. Exp.*, vol. 25, no. 21, pp. 26133–26147, Oct. 2017.

[27] W. Wang, M. Zhang, S. Yan, Z. Fan, and J. Tan, "Absolute spherical surface metrology by differencing rotation maps," *Appl. Opt.*, vol. 54, no. 20, pp. 6186–6189, Jul. 2015.

[28] Y. Liu, L. Miao, W. Zhang, C. Jin, and H. Zhang, "Extended shift-rotation method for absolute interferometric testing of a spherical surface with pixel-level spatial resolution," *Appl. Opt.*, vol. 56, no. 16, pp. 4886–4891, Jun. 2017.